Available online at www.sciencedirect.com
ScienceDirect
Journal of Magnetic Resonance 190 (2008) 298–306
JMR Journal of Magnetic Resonance
www.elsevier.com/locate/jmr

Accurate measurements of small *J* coupling constants under inhomogeneous fields via intermolecular multiple-quantum coherences

Yanqin Lin [a], Zhong Chen [a,b,*], Shuhui Cai [a], Jianhui Zhong [b,*]

[a] *Department of Physics, State Key Laboratory for Physical Chemistry of Solid Surface, Xiamen University, Xiamen, Fujian 361005, PR China*
[b] *Department of Radiology, University of Rochester, Rochester, NY 14642, USA*

Received 6 September 2007; revised 12 November 2007
Available online 22 November 2007

Abstract

Two new NMR pulse sequences, based on intermolecular multiple-quantum coherences (iMQCs), were developed to obtain apparent *J* coupling constants with a scaling factor from one to infinity relative to the conventional *J* coupling constants. Here the apparent *J* coupling constants were defined as apparent peak separations in unit of Hz in a reconstructed spectrum for a coupled spin system. Except for the adjustable scaling factor for apparent *J* coupling constants, the sequences hold the advantage of high acquisition efficiency, and retain the spectral information such as chemical shifts, multiplet patterns, and relative peak areas under inhomogeneous fields. For spin systems with small scalar coupling constants, well-resolved *J*-spectra can be achieved by selecting a proper scaling factor. Theoretical predictions are in good agreement with simulation results and experimental observations.

Keywords: High-resolution NMR spectra; Intermolecular multiple-quantum coherences; Inhomogeneous fields; Apparent *J* coupling constant; Scaling factor

1. Introduction

High-resolution nuclear magnetic resonance (NMR) spectra can provide useful information of chemical shifts, *J* coupling constants, multiplet patterns, and relative peak areas for structure identification. For conventional high-resolution liquid NMR experiments, the homogeneity of magnetic field exceeding 10^{-8} is often required. However, there are many circumstances where homogeneity of the magnetic field is degraded due to intrinsic variation in magnetic susceptibility at the interface of various structural components over a sample volume, such as heterogeneous tissues in human or animal *in vivo* NMR, rock samples for oil exploration and porous resin beads in combinational chemistry. These field inhomogeneities often cannot be completely eliminated with a conventional field shimming method. Variation in spatial and temporal homogeneity of the magnetic field may produce spurious field gradients which will broaden resonance lines and obscure fine spectral features.

Besides recent improvements in shimming techniques [1,2], many methods have been developed to address the above problem and to extract high-resolution NMR information from spectra acquired in inhomogeneous magnetic fields. Blümich and co-workers developed a unilateral and mobile NMR sensor for high-resolution NMR spectra at low magnetic field strengths [3,4]. More recently, a method to obtain high-resolution spectroscopy of rat brain *in vivo* was proposed via detecting intra-molecular zero-quantum coherence [5]. Although these techniques can partially remove inhomogeneous broadening, they cannot provide

* Corresponding authors. Address: Department of Physics, Xiamen University, Xiamen, Fujian 361005, PR China. Fax: +86 592 2189426.
E-mail addresses: chenz@xmu.edu.cn (Z. Chen), jianhui.zhong@rochester.edu (J. Zhong).

1090-7807/$ - see front matter © 2007 Elsevier Inc. All rights reserved.
doi:10.1016/j.jmr.2007.11.010

correct multiplet patterns and relative peak areas. In the past 10 years, intermolecular multiple-quantum coherences (iMQCs) caused by long-range dipolar interactions have generated tremendous interests [6–9]. Sequences based on iMQCs among spins in different molecules were designed to obtain high-resolution information, such as chemical shifts, J coupling constants, multiplet patterns and relative peak areas, under inhomogeneous fields. Since intermolecular dipolar interactions are effective in the range of 5–500 μm which is far smaller than typical sample dimensions, it is intuitively attractive for NMR spectroscopy in inhomogeneous fields. Warren and co-workers proposed a few pulse sequences based on intermolecular zero-quantum coherences (iZQCs): HOMOGENIZED (HOMOGeneity ENhancement in Intermolecular ZEro-quantum Detection) [10], composite CPMG-HOMOGENIZED [11], and ultrafast iZQC 2D spectroscopy technique [12]. We have also designed some pulse sequences based on iZQCs and intermolecular double quantum coherences (iDQCs), including SEL-HOMOGENIZED (SELective HOMOGENIZED) [13] and IDEAL (Intermolecular Dipolar-interaction Enhanced All Lines) [14]. Recently, Faber and co-workers proposed some sequences similar to SEL-HOMOGENIZED [15,16]. Although all these schemes [10–13,15,16] can retain useful spectral information, the obtained apparent J coupling constants, defined as apparent peak separations in unit of Hz in a reconstructed spectrum for a coupled spin system, remain the same value as conventional J coupling constants except for IDEAL [14], with which the apparent J coupling constants were obtained with a scaling factor (SF) of 3 relative to the conventional J coupling constants. Therefore, these schemes may not be suitable for accurate measurements of scalar coupling constants for the spin systems with small J coupling constants under inhomogeneous fields.

The importance of accurate J coupling constants has long been recognized. Some *in vivo* spectroscopists pay their attention to obtain exact values of J coupling constants and chemical shifts, which are required for spectral fitting in *in vivo* spectral analysis. However, not all J coupling constants (especially small J coupling constants) are known under *in vivo* conditions. Moreover, J coupling constants and chemical shifts may vary from *in vitro* to *in vivo* due to the changes of molecular environment, cation binding, temperature, ionic strength and pH, etc [5]. In addition, it is hard, even impossible, to acquire accurate values in many other cases, especially for systems with small coupling constants close to the value of the spectral linewidth. Some pulse sequences, data processing methods and special devices were developed to evaluate coupling constants. Based on conventional single-quantum coherences (SQCs) or intramolecular multiple quantum coherences, several pulse sequences, such as MJ-HMQC and MJ-HSQC, were designed to obtain apparent J coupling constants with a scaling factor for precisely measuring the constants of several Hertz in homogeneous fields [17–19]. Sequences to obtain selective J-resolved spectra, which can reveal mutual couplings between single spin pairs, were proposed to obtain accurate homonuclear coupling constants [20,21]. These sequences are, however, not suitable for obtaining simultaneously the useful spectral information, such as chemical shifts, J coupling constants, multiplet patterns, and relative peak areas in inhomogeneous fields. On the other hand, the data processing methods for measuring small J coupling constants [22–24], such as J-doubling and ACCA (Automatic Coupling Constants Analyzer), require high quality experimental spectra with well-resolved and baseline-corrected multiplets, which is difficult to obtain in inhomogeneous fields. In nanotesla magnetic fields, heteronuclear J coupling constants are obtained using special equipments, such as superconducting quantum interference device (SQUID) sensors, in the absence of chemical shifts [25].

The purpose of present work is to design new pulse sequences with which to obtain apparent homonuclear J coupling constants with a scaling factor in a large range while retaining the conventional high-resolution spectral information of chemical shifts, multiplet patterns, and relative peak areas for various spin systems and/or in inhomogeneous fields. The new sequences, named J-scaling iMQC-1 and J-scaling iMQC-2, respectively, are devised based on iMQC acquisitions with three evolution periods and three gradient pulses. Theoretically they can provide a scaling factor for apparent J coupling constants ranging from one to infinity, selected optimally for a specific spin system to obtain the precise values of conventional J coupling constants. Moreover, the new sequences are highly time-efficient with narrow spectral width sampled in the indirect dimension.

2. Theoretical formalism

The designed pulse sequences of J-scaling iMQC-1 and J-scaling iMQC-2 are shown in Fig. 1. The variable m in

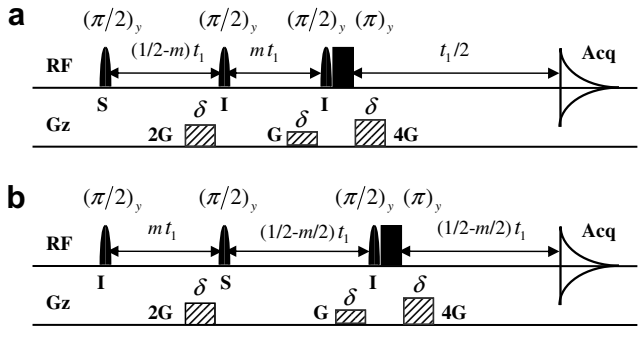

Fig. 1. J-scaling pulse sequences for high-resolution spectra in inhomogeneous fields via intermolecular multiple coherences. (a) J-scaling iMQC-1, SF $\geqslant 3$ with $0 < m \leqslant 1/2$, (b) J-scaling iMQC-2, $1 \leqslant \mathrm{SF} \leqslant 3$ with $0 \leqslant m \leqslant 1$. Full vertical bars stand for non-selective RF pulses. Gauss-shaped pulses are frequency-selective, with the three selective RF pulses exciting S, I, and I components, respectively, (indicated by S, I, and I under each pulse). The phases of the RF pulses are indicated by subscripts. The dash rectangles stand for correlation gradients.

J-scaling iMQC-1 is limited in the range of $0 < m \leqslant 1/2$, while it is $0 \leqslant m \leqslant 1$ in J-scaling iMQC-2. A homogeneous liquid mixture is taken as an example, which consists of an AX spin-1/2 system of S component (including S_k and S_l spins with a scalar coupling constant J_{kl}) and a single spin-1/2 system of I component. It is assumed that the I component (corresponding to solvent) is abundant and S component (corresponding to solute) is either abundant or dilute. Assume that Ω_q is the frequency offset of spin q ($q = I$, S_k, S_l) in the rotating frame in the absence of field inhomogeneity, and $\Delta B(\boldsymbol{r})$ is the inhomogeneous field at position $\boldsymbol{r}$. When the spatial position-dependent magnetic field is taken into account, the frequency offset, $\Omega_q(\boldsymbol{r})$, of the q spin at position $\boldsymbol{r}$ is given by

$$\Omega_q(r) = \omega_q + \gamma \cdot \Delta B(r), \quad (q = I, S_k, S_l), \tag{1}$$

where γ is the gyromagnetic ratio. Eq. (1) suggests that the magnetic field inhomogeneity causes a shift of angular frequency from the resonance frequency ω_q.

In the following, theoretical expressions of the spin evolutions under the pulse sequences of J-scaling iMQC-1 will be derived from the iMQC treatment. For simplification, the effects of radiation damping, diffusion, relaxation, and intermolecular nuclear Overhauser effect (NOE) are ignored, and the correlation gradients are applied along z direction. For J-scaling iMQC-1, the three selective radio-frequency (RF) pulses excite S, I, and I components respectively (indicated by S, I, and I under each pulse). The first selective $(\pi/2)_y^S$ RF pulse rotates the magnetization density of S component into the transverse plane. After dropping unimportant factors and terms, we can express the single-quantum term $I_z S_{kx}$ in the reduced density operator using raising and lowering operators,

$$\sigma(0^+) = \sum_{i=1}^{N_S}\sum_{j=1}^{N_I} I_{zj} S_{kxi} = \sum_{i=1}^{N_S}\sum_{j=1}^{N_I} \frac{1}{2} I_{zj} S_{ki}^+ + \frac{1}{2} I_{zj} S_{ki}^-, \tag{2}$$

where S_{kxi} represents the x component of the i-th spin S_k operator, I_{zj} represents the z component of the j-th spin I operator, and N_S and N_I are the molecular numbers of the solute (S component) and solvent (I spin) respectively. The spin density operators evolve under the chemical shift, scalar coupling, and magnetic field gradient during the first evolution period $(0.5 - m)t_1$. It is well known that all density operator components except coherence order $p = -1$ are unobservable and can be disregarded during the detection period [26]. In the case of J-scaling iMQC-1, only the term $I_z S_{ki}^+$ in Eq. (2) is chosen by the correlation gradients. We have

$$\begin{aligned}\sigma[(0.5-m)t_1^-] = \sum_{i=1}^{N_S}\sum_{j=1}^{N_I} \frac{1}{2} I_{zj}\{&S_{ki}^+ \cos[\pi J_{kl}(0.5-m)t_1] \\ &- \mathrm{i}2 S_{ki}^+ S_{lzi} \sin[\pi J_{kl}(0.5-m)t_1]\}\mathrm{e}^{-\mathrm{i}[2\varphi(r_i)]} \\ &\times \mathrm{e}^{-\mathrm{i}[\Omega_{S_{ki}}(r_i)](\frac{1}{2}-m)t_1}.\end{aligned} \tag{3}$$

The phase angle at positions $\boldsymbol{r}_i$ for S_{ki}^+ due to the first correlation gradient is $2\varphi(\boldsymbol{r}_i) = 2\gamma G \delta s_i$, where s_i is the locations of the i-th spin S_k along the gradient direction $\boldsymbol{s}$. The second selective $(\pi/2)_y^I$ RF pulse converts I_{zj} into $(0.5I_j^+ + 0.5I_j^-)$, and only the double-quantum terms are chosen by the correlation gradients. We have

$$\begin{aligned}\sigma[(0.5-m)t_1^+] = \sum_{i=1}^{N_s}\sum_{j=1}^{N_I} \frac{1}{4} I_j^+\{&S_{ki}^+ \cos[\pi J_{kl}(0.5-m)t_1] \\ &- \mathrm{i}2 S_{ki}^+ S_{lzi} \sin[\pi J_{kl}(0.5-m)t_1]\} \\ &\times \mathrm{e}^{-\mathrm{i}[2\varphi(r_i)]}\mathrm{e}^{-\mathrm{i}[\Omega_{s_{ki}}(r_i)](\frac{1}{2}-m)t_1}.\end{aligned} \tag{4}$$

The spin density operators evolve under the chemical shift, scalar coupling, and magnetic field gradient during the second evolution period mt_1.

$$\begin{aligned}\sigma\left(\frac{1}{2}t_1^-\right) = \sum_{i=1}^{N_s}\sum_{j=1}^{N_I} \frac{1}{4} I_j^+[&S_{ki}^+ \cos(\pi J_{kl} t_1/2) - i2 S_{ki}^+ S_{lzi} \\ &\times \sin(\pi J_{kl} t_1/2)]\mathrm{e}^{-\mathrm{i}[3\varphi(r_i)+\varphi(r_j)]}\mathrm{e}^{-\mathrm{i}[\Omega_{S_{ki}}(r_i)]\frac{1}{2}t_1}\mathrm{e}^{-\mathrm{i}[\Omega_{I_j}(r_j)]mt_1}.\end{aligned} \tag{5}$$

The phase angle at position $\boldsymbol{r}_j$ for I_j^+ due to the correlation gradient is $\varphi(\boldsymbol{r}_j) = \gamma G \delta s_j$, where s_j is the locations of the j-th spin I along the gradient direction $\boldsymbol{s}$. The third selective $(\pi/2)_y^I$ RF pulse converts I_j^+ into $(0.5I_j^+ - 0.5I_j^- - I_{zj})$. The fourth non-selective $(\pi)_y$ RF pulse flips the coherence order from $S_{ki}^+ I_{zj}$ to $S_{ki}^- I_{zj}$. Since there are no subsequence pulses, we only need to consider the SQC terms which contribute to the observable signal. We have

$$\begin{aligned}\sigma\left(\frac{1}{2}t_1^+\right) = \sum_{i=1}^{N_S}\sum_{j=1}^{N_I} \frac{1}{4} I_{zj}\{&S_{ki}^- \cos(\pi J_{kl} t_1/2) + \mathrm{i}2 S_{ki}^- S_{lzi} \\ &\times \sin(\pi J_{kl} t_1/2)\}\mathrm{e}^{-\mathrm{i}[3\varphi(r_i)+\varphi(r_j)]}\mathrm{e}^{-\mathrm{i}[\Omega_{S_{ki}}(r_i)]\frac{1}{2}t_1}\mathrm{e}^{-\mathrm{i}[\Omega_{I_j}(r_j)]mt_1}.\end{aligned} \tag{6}$$

When the magnetic field gradient, chemical shift, dipolar coupling, and scalar coupling are all taken into account during the period $t_1/2 + t_2$, the observable signal at the detection period can be written as

$$\begin{aligned}\sigma(t_1+t_2) = -\frac{i}{8}\sum_{i=1}^{N_S}\sum_{j=1}^{N_I} &S_{ki}^- \cos[\pi J_{kl}(t_1+t_2)] \\ &\times \sin\left[1.5 D_{ij}\left(\frac{1}{2}t_1 + t_2\right)\right] \\ &\times \mathrm{e}^{-\mathrm{i}[-\varphi(r_i)+\varphi(r_j)]}\mathrm{e}^{\mathrm{i}[\Omega_{S_{ki}}(r_i)]t_2}\mathrm{e}^{-\mathrm{i}[\Omega_{I_j}(r_j)]mt_1},\end{aligned} \tag{7}$$

where D_{ij} is the residual intermolecular dipolar coupling constant. Since D_{ij} is very small in a usual case, we have $\sin[1.5D_{ij}(0.5t_1 + t_2)] \approx 1.5D_{ij}(0.5t_1 + t_2)$ when $1.5D_{ij}(0.5t_1 + t_2) \ll 1$. Therefore, Eq. (7) can be simplified to

$$\begin{aligned}\sigma(t_1+t_2) = -\frac{3\mathrm{i}}{16}\left(\frac{1}{2}t_1 + t_2\right)\sum_{i=1}^{N_S}\sum_{j=1}^{N_I} &S_{ki}^- \cos[\pi J_{kl}(t_1+t_2)] \\ &\times D_{ij}\mathrm{e}^{-\mathrm{i}[-\varphi(r_i)+\varphi(r_j)]}\mathrm{e}^{\mathrm{i}[\Omega_{S_{ki}}(r_i)]t_2}\mathrm{e}^{-\mathrm{i}[\Omega_{I_j}(r_j)]mt_1}.\end{aligned} \tag{8}$$

For simplicity, only the case of an isotropic sample will be considered under a small linear inhomogeneous magnetic field along the direction of the correlation gradients. We have

$$\sigma(t_1+t_2)=\frac{(0.5t_1+t_2)\mathrm{i}\Delta_s}{16\tau_d^I}\left(\frac{kT}{\hbar\omega_I}\right)M_{S_k}^-\{\mathrm{e}^{-\mathrm{i}[m\omega_I-\pi J_{kl}]t_1}\times e^{i[\omega_{S_k}+\pi J_{kl}]t_2}+\mathrm{e}^{-\mathrm{i}[m\omega_I+\pi J_{kl}]t_1}\mathrm{e}^{\mathrm{i}[\omega_{S_k}-\pi J_{kl}]t_2}\}, \quad (9)$$

where $\frac{kT}{\hbar\omega_I}$ is the reciprocal of Boltzmann factor; $\tau_d^I\equiv\frac{1}{\gamma\mu_0 M_0^I}$, is the dipolar demagnetizing time, in which M_0^I is the magnetization of spin I, μ_0 is the vacuum permeability; and $\Delta_s\equiv\frac{[3(\hat{s}\cdot\hat{z})^2-1]}{2}$.

Eq. (9) shows that the centers of intermolecular cross-peaks in the resulting 2D NMR spectrum locate at $(m\omega_I-\pi J_{kl},\omega_{S_k}+\pi J_{kl})$ and $(m\omega_I+\pi J_{kl},\omega_{S_k}-\pi J_{kl})$, respectively. If the frequency offset of I spin is set to zero, i.e. $\Omega_I=0$, the intermolecular cross peaks between the I and S spins will center at $(-\pi J_{kl},\omega_{S_k}+\pi J_{kl})$ and $(\pi J_{kl},\omega_{S_k}-\pi J_{kl})$. Eq. (9) implies that all the streaks in the 2D spectrum occupy only a narrow range of frequency in the F1 dimension. This enables a substantial decrease of the F1 spectral width that needs to be sampled, and greatly reduces experimental time and data space. From Eq. (9), it also can be seen that all steaks lie along the direction $\phi=\mathrm{arctg}(m)$, where ϕ is the angle of spectral peaks relative to the F2 axis. This indicates that using J-scaling iMQC-1, the apparent J coupling constants will be obtained with a scaling factor $SF=1+\frac{1}{m}$ with $0<m\leqslant\frac{1}{2}$ when the streaks are projected onto the F2 dimension after a counterclockwise rotation of $\pi/2-\phi$.

When the J-scaling iMQC-2 pulse sequence is employed, the resulting signal of the same sample can be deduced similarly. The observable signal at the detection period can be expressed as

$$\sigma(t_1+t_2)=\frac{(0.5t_1+t_2)\mathrm{i}\Delta_s}{16\tau_d^I}\left(\frac{kT}{\hbar\omega_I}\right)M_{S_k}^-\{\mathrm{e}^{-\mathrm{i}[\frac{1+m}{2}\omega_I-\pi J_{kl}(1-m)]t_1}\times\mathrm{e}^{\mathrm{i}(\omega_{S_k}+\pi J_{kl})t_2}+\mathrm{e}^{-\mathrm{i}[\frac{1+m}{2}\omega_I+\pi J_{kl}(1-m)]t_1}\times\mathrm{e}^{\mathrm{i}(\omega_{S_k}-\pi J_{kl})t_2}\}. \quad (10)$$

Eq. (10) shows that the centers of the intermolecular cross-peaks appear at $(\frac{1+m}{2}\omega_I-(1-m)\pi J_{kl},\omega_{S_k}+\pi J_{kl})$ and $(\frac{1+m}{2}\omega_I+(1-m)\pi J_{kl},\omega_{S_k}-\pi J_{kl})$, respectively. If the frequency offset of I spin is set to zero, i.e. $\Omega_I=0$, the intermolecular cross-peaks between I and S spins then center at $(-(1-m)\pi J_{kl},\omega_{S_k}+\pi J_{kl})$ and $((1-m)\pi J_{kl},\omega_{S_k}-\pi J_{kl})$. Similar to J-scaling iMQC-1, a narrow F1 spectral width can satisfy the experimental requirement when J-scaling iMQC-2 is employed. From Eq. (10), it can be seen that all streaks lie along the direction $\phi=\mathrm{arctg}(\frac{1+m}{2})$, where ϕ is the angle of spectral peaks with respect to the F2 axis. Projecting the streaks onto the F2 dimension after a counterclockwise rotation of $\pi/2-\phi$, the scaling factor for apparent J coupling constant in resulting spectrum is given by: $SF=\frac{3-m}{1+m}$ with $0\leqslant m\leqslant 1$.

The above analysis suggests that although the two sequences in Fig. 1 employ the same number of selective $\pi/2$ pulses, non-selective π pulse, and gradient pulses, the difference in their positions (i.e. the time they are applied) results in different apparent J coupling constants: the scaling factor ranges from three to infinity for J-scaling iMQC-1, and from one to three for J-scaling iMQC-2. With these two sequences, a well-resolved J-spectrum for system with small scalar coupling constants can be achieved by selecting an optimal scaling factor while retaining the conventional spectral information of chemical shifts, J coupling constants, multiplet patterns, and relative peak areas.

3. Experiments and simulations

All experiments were performed at 298 K using a 500 MHz Varian NMR System spectrometer and a 5 mm indirect detection probe with three-dimension gradient coils. In order to test the scaling ability of the proposed pulse sequences for apparent scalar coupling constants, a sample of mixture of methyl ethyl ketone (MEK, $CH_3COCH_2CH_3$) and cyclohexane (C_6H_{12}) was used. About 25% (by volume) acetone-d_6 was added to the sample for field lock and shimming as well as for reducing the effects of radiation damping. The gradient with strength G of 0.05 T/m and duration δ of 1.2 ms was applied. To further suppress the radiation damping during the evolution and detection periods, the width of the $\pi/2$ hard RF pulse was extended to 67 μs by deliberately detuning the probe. Although detuning the probe also causes signal loss, it is necessary for suppressing the radiation damping effects which influence the detection of iMQC signal. The selective $\pi/2$ Gaussian pulse for solvent had a width of 9.4 ms and was frequency selective for the solvent peak. The pulse for the selection of solute consists of a $\pi/2$ hard pulse and a selective $\pi/2$ pulse with an opposite phase for solvent. The spectral width of F1 dimension was 50 Hz in 30 increments, and was 1200 Hz for F2 dimension. The pulse repetition time was 3.0 s and the acquisition time t_2 was 0.6 s. The total experimental time was about 2 min. The signal was zero filling to 512×4096 before a regular FFT process.

The ability of the proposed pulse sequences for enhancing spectral resolution in systems with small J coupling constants was tested using a sample of histidine aqueous solution. D_2O was added to the sample for field lock and shimming as well as for reducing the effects of radiation damping. The gradient with strength G of 0.04 T/m and duration δ of 1.2 ms was applied. The width of the RF $\pi/2$ hard pulse was extended to 19 μs by deliberately detuning the probe. The selective $\pi/2$ Gaussian pulse for solvent had a width of 5.8 ms and was frequency selective on the solvent peak. The spectral width of F1 dimension was 60 Hz in 90 increments, and was 3200 Hz for F2 dimension. The pulse repetition time was 6.0 s and the acquisition time t_2 was 0.3 s. The total experimental time was about 11 min. The signal was zero filling to 1024×8192 before a regular FFT process. All the acquired 1D spectra are displayed in the phase mode while 2D spectra and their 1D projections in the magnitude mode.

In order to verify the theoretical predictions and experimental observations, the modified Bloch equations were used to simulate 2D spectra of a mixture of methyl ethyl ketone and cyclohexane based on a simulation algorithm

presented previously [27]. The parameters for the simulations were chosen to be as close to the experimental ones as possible.

4. Results and discussion

Spectra of methyl ethyl ketone and cyclohexane are shown in Figs. 2–4. Conventional 1D spectrum of the sample in a homogeneous magnetic field was first acquired, as shown in Fig. 2a. The magnetic field was then intentionally deshimmed to produce a linewidth of ~30 Hz (phase mode). The resulting 1D spectrum is illustrated in Fig. 2b. The 2D spectra from *J*-scaling iMQC-1 sequence with $m = 1/4$ and *J*-scaling iMQC-2 sequence with $m = 1/3$ were acquired and simulated under the same inhomogeneous field. The results are shown in Figs. 3 and 4. The projection of Fig. 3a onto the F2 dimension after a counterclockwise rotation of 75.96° is shown in Fig. 2c, and the projection of Fig. 4a after a counterclockwise rotation of 56.31° is shown in Fig. 2d. The corresponding simulated results are shown in Fig. 2e and f. It can be seen that the projected spectra maintain chemical shifts, relative peak areas, and multiplet patterns while inhomogeneous broadening is suppressed. Moreover, the *J* splitting distances are apparently 5-fold magnified in Fig. 2c and e and 2-fold magnified in Fig. 2d and f compared to Fig. 2a, which agree well with the theoretical predictions. An apparent magnification of *J* splits allows more accurate measurement of small *J* coupling constants. Since *J* splitting distances obtained with these sequences are SF times of the conventional ones, appropriate relations between SF and time delay factor *m* need to be used for calculating the true *J* values, as discussed in the *Theoretical Formalism* section.

As mentioned earlier, all the streaks in the 2D spectra from the pulse sequences in Fig. 1 align along the center of the F1 dimension. This enables a substantial decrease of the F1 spectral width that needs to be sampled, and leads to reduced experimental time, data size, and data processing time.

Since the SF $\geqslant 1$ for both sequences, they are suitable for weakly coupled spin systems. The *J*-scaling iMQC-1 sequence with scaling factor in the range of three to infinity is especially suitable for extremely weakly coupled spin systems. The parameter *m* can be determined depending upon the spectral features to achieve an optimal result. Since large scaling factor may lead to overlap of spectral peaks, $SF = 1$ may be the best choice for strongly coupled spin systems.

The linewidth in the indirect dimension of an iMQC spectrum depends on several factors including transverse relaxation, diffusion, inhomogeneous fields in the dipolar correlation distance, and dipolar field. It is difficult, even impossible, to obtain a quantitative relationship between all these factors and linewidth. The linewidth of the reconstructed 1D high-resolution spectrum will increase with the increase of scaling factor. However, increase of the linewidth is at a slower rate than that of the scaling factor. Therefore, the spectral resolution enhances as a whole even in the presence of field imhomogeneity.

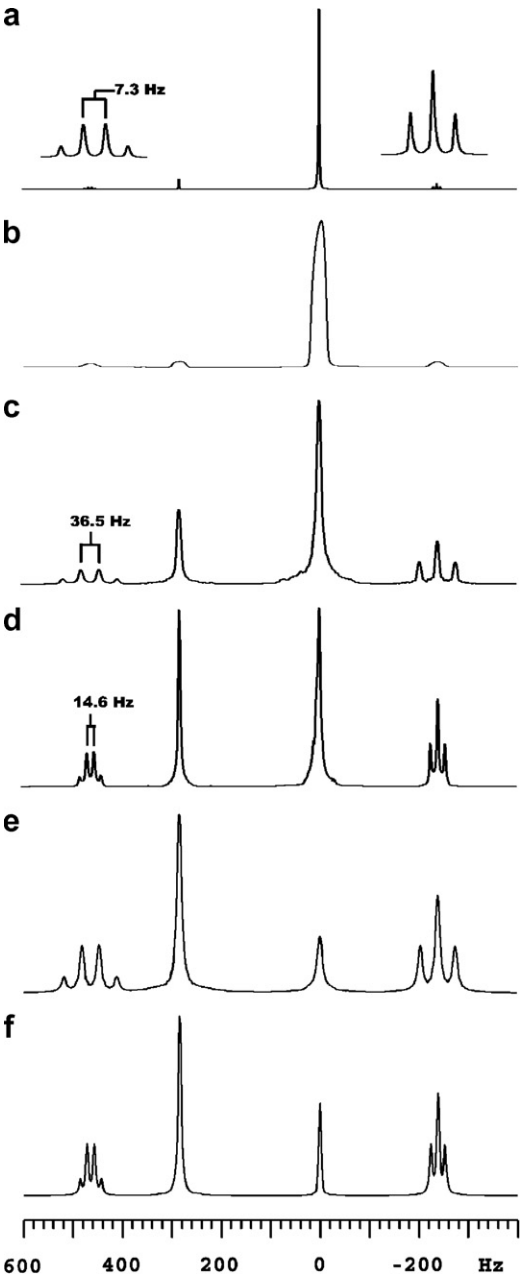

Fig. 2. 1D ^{1}H NMR spectra of the mixture of methyl ethyl ketone ($CH_3COCH_2CH_3$) and cyclohexane (C_6H_{12}). (a) Conventional 1D high-resolution spectrum acquired in a well-shimmed field, (b) 1D spectrum in an inhomogeneous field of about 30 Hz linewidth (phase mode), (c) accumulated projection of the sheared experimental spectrum shown in Fig. 3b, (d) accumulated projection of the sheared experimental spectrum shown in Fig. 4b, (e) accumulated projection of the sheared simulation spectrum shown in Fig. 3d, and (f) accumulated projection of the sheared simulation spectrum shown in Fig. 4d. Insets are magnified in both vertical and horizontal directions.

Experimental results of histidine aqueous solution are shown in Figs. 5 and 6, for testing the ability of *J*-scaling iMQC-1 in differentiating spin systems with small *J* coupling constants. The structure of histidine is given on the

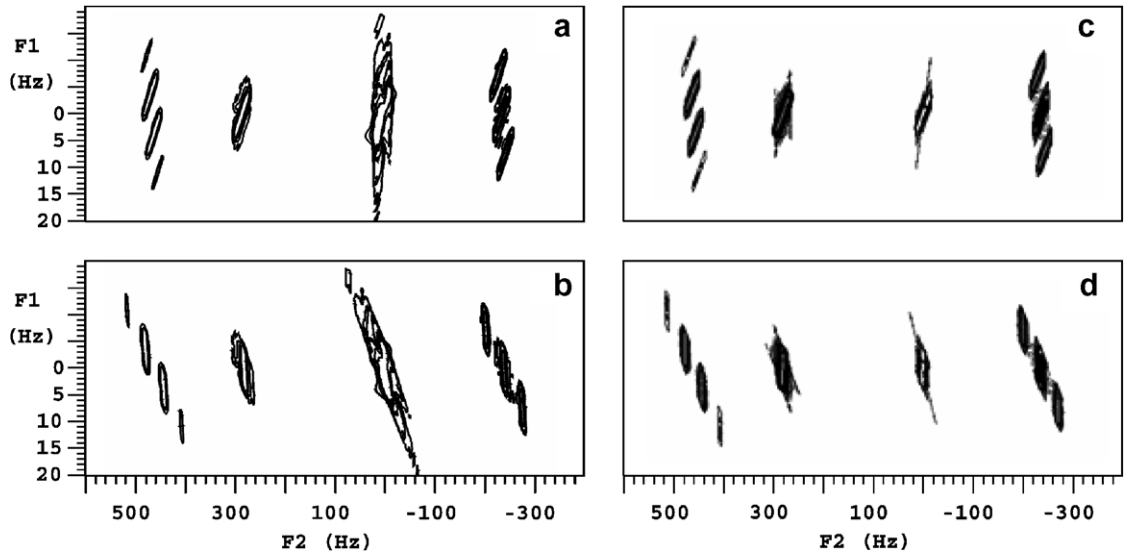

Fig. 3. 2D ^{1}H NMR spectra of the mixture of methyl ethyl ketone and cyclohexane using the *J*-scaling iMQC-1 pulse sequence in the same inhomogeneous field as Fig. 2b. (a) Experimental spectrum with $m = 1/4$, (b) sheared spectrum of (a) after a counterclockwise rotation of 75.96°, (c) simulated spectrum corresponding to (a), and (d) simulated spectrum corresponding to (b).

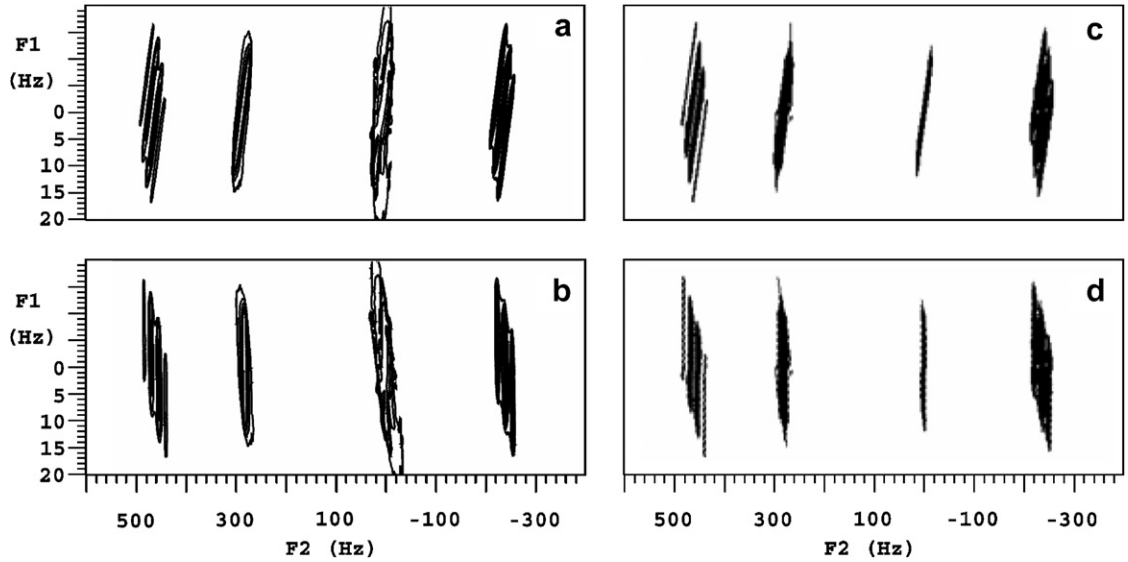

Fig. 4. 2D ^{1}H NMR spectra of the mixture of methyl ethyl ketone and cyclohexane using the *J*-scaling iMQC-2 pulse sequence in the same inhomogeneous field as Fig. 2b. (a) Experimental spectrum with $m = 1/3$, (b) sheared spectrum of (a) after a counterclockwise rotation of 56.31°, (c) simulated spectrum corresponding to (a), and (d) simulated spectrum corresponding to (b).

top left of Fig. 5. There are five multiplets in its ^{1}H NMR spectrum (denoted as A, B, C, D and E) using conventional single-pulse sequence as shown in Fig. 5a. Scalar couplings exist between A and B, B and D, B and E, C and D, C and E, and D and E. The coupling constants J_{AB}, J_{BD} and J_{BE} are small, while J_{CD}, J_{CE} and J_{DE} are large. Fig. 5a shows that the *J* coupling information is limited even though the sample is placed in a well-shimmed magnetic field. Fig. 5b shows that all the *J* coupling information is vanished under an inhomogeneous field of about 30 Hz linewidth (phase mode). Fig. 6a displays the 2D spectrum obtained from *J*-scaling iMQC-1 with $m = 1/10$ under the same inhomogeneous field as Fig. 5b. Fig. 6b shows the sheared spectrum of Fig. 6a after a counterclockwise rotation of 84.29°. The multiplet of A appears as a well-resolved doublet in Fig. 6, which cannot be resolved well even in a well-shimmed field (see Fig. 5a), and J_{AB} can be obtained from projection onto the F2 dimension. Although the multiplet

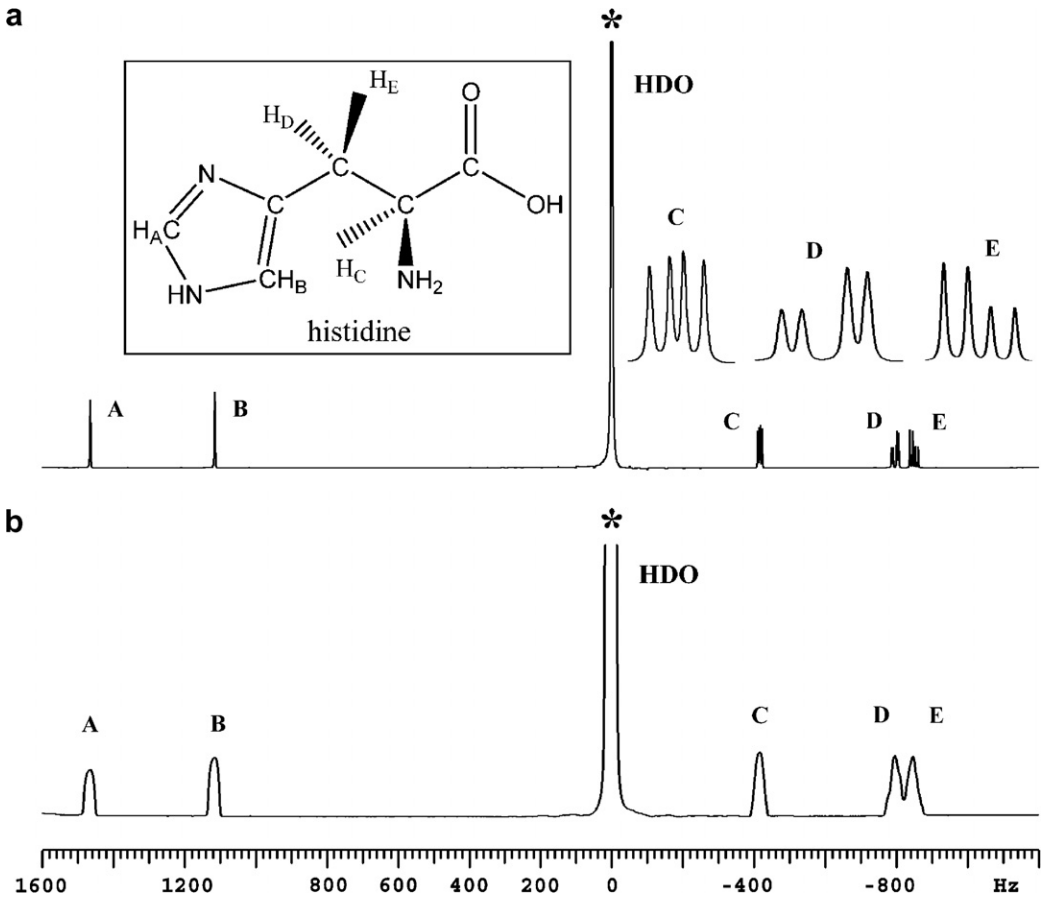

Fig. 5. 1D ^{1}H NMR spectra of histidine aqueous solution. (a) Conventional 1D high-resolution spectrum acquired in a well-shimmed field, and (b) 1D spectrum in an inhomogeneous field of about 30 Hz linewidth (phase mode). The peaks marked by * are truncated due to their strong intensities. Insets are magnified in both vertical and horizontal directions. The structure of histidine is shown in the block on the top left.

of B is not well resolved in Fig. 6, the J coupling constants J_{AB}, J_{BD} and J_{BE} can be measured from the multiplets of A, D and E, respectively. The resolution of multiplet C in Fig. 6 is much better than that in Fig. 5a. The eight splitting peaks are clearly seen for the multiplets D and E. Although some J coupling constants still cannot be obtained from the accumulated projection, they can be acquired directly from the 2D spectrum of Fig. 6b. The distance between lines 1 and 2 is 11 times of the value of J_{BD}, and the distance between lines 3 and 4 is 11 times of the value of J_{BE} (see expanded region of D and E in Fig. 6b).

For comparison, a conventional homonuclear 2D J-resolved spectrum of the histidine aqueous solution with water pre-saturation under a homogeneous field (data not shown) was measured. The results obtained from J-scaling iMQC-1, $J_{AB} = 1.38$ Hz, $J_{BD} = 1.09$ Hz, $J_{BE} = 0.91$ Hz, $J_{CD} = 4.74$ Hz, $J_{CE} = 8.00$ Hz, and $J_{DE} = 15.47$ Hz, are in excellent agreement with those obtained from the 2D J-resolved spectrum, $J_{AB} = 1.40$ Hz, $J_{BD} = 1.04$ Hz, $J_{BE} = 0.89$ Hz, $J_{CD} = 4.74$ Hz, $J_{CE} = 7.99$ Hz, and $J_{DE} = 15.48$ Hz. It is noted that the J-scaling iMQC-1 method has the advantage that it can be used to obtain high-resolution 1D spectra under inhomogeneous fields, which cannot be realized using the conventional 2D J-resolved method. Compared to the J coupling constants ($J_{CD} = 4.81$ Hz, $J_{CE} = 7.96$ Hz, $J_{DE} = 15.51$ Hz, $J_{A\text{-}NH} = 1.07$ Hz, $J_{B\text{-}NH} = 1.20$ Hz and $J_{BD} = J_{BE} = 0.72$ Hz) reported previously [28], the three sets of J_{CD}, J_{CE}, and J_{DE} values agree well with each other. However, the values and/or assignments of the small J coupling constants of $J_{A\text{-}NH}$, $J_{B\text{-}NH}$, J_{BD}, and J_{BE} reported in reference [28] are different from those obtained from the conventional 2D J-resolved and J-scaling iMQC-1 results. This may be because histidine sample of a slightly different composition was used and/or the 1D measurements were not performed under ideal conditions such as with appropriate shimming and sensitivity in the reference [28]. To further verify our assignments, we also performed a long-range H-H COSY experiment under a homogeneous field (data not shown). The result indicates that proton A couples with proton B. This is different from the assignment that proton A couples with the proton of the NH group in reference [28].

Incomplete revelation of the eight peaks of multiplet B as seen in Fig. 6 is probably due to the fact that the relation $J_{BD} + J_{BE} > J_{AB}$ (J_{AB} is the largest J coupling constants

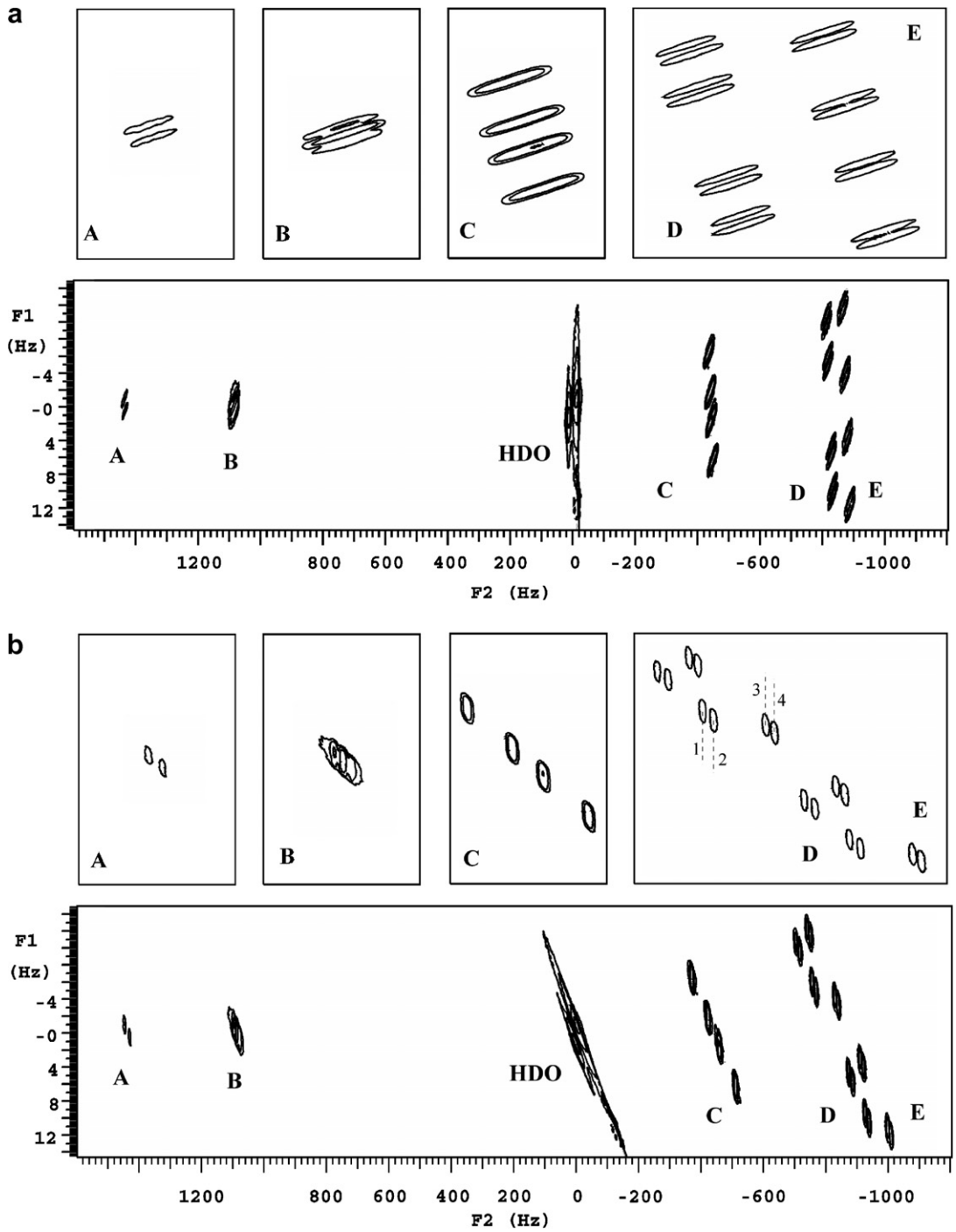

Fig. 6. 2D ^{1}H NMR spectra of histidine aqueous solution using the *J*-scaling iMQC-1 pulse sequence with $m = 1/10$ in the same inhomogeneous field as Fig. 5b. (a) Experimental spectrum, (b) sheared spectrum of (a) after a counterclockwise rotation of 84.29°. Regions A, B, C, D, and E are magnified in both vertical and horizontal directions in both (a) and (b).

among these three small *J* coupling constants) results in overlapping of the eight splitting peaks.

It is important to determine the scaling factor by choosing a proper value for parameter *m*. If the scaling factor is too small, the splitting of resonances may not be measured accurately. For the histidine aqueous solution, eight splitting peaks of multiplet E would be difficult to resolve if parameter *m* was set to 1/5 (data not shown). On the other hand, an excess large scaling factor is not desired either because overlap of spectral peaks will aggravate under this condition. For an unknown sample, a small scaling factor for assignment of the spectral peaks and a big scaling factor for splitting condition may be needed, and an optimal parameter *m* (scaling factor) should be selected accordingly.

5. Conclusions

Two new pulse sequences, *J*-scaling iMQC-1 and *J*-scaling iMQC-2, with three selective RF pulses and three gradient pulses were devised to obtain apparent *J* coupling constants with a scaling factor in the range of one to infinity for high-resolution spectra in inhomogeneous fields with 2D acquisitions. The intermolecular MQC treatment was utilized to derive analytical expressions of signals. Compared to the existing pulse sequences for high-resolution spectra in inhomogeneous fields, the new sequences are suitable for various kinds of weakly and moderately strongly coupled spin systems to achieve a better resolution while retaining the conventional spectral information including chemical shifts, *J* coupling constants, multiplet patterns, and relative peak areas. All experimental observations and simulated results are in excellent agreement with the theoretical predictions. In view of the ability of obtaining apparent *J* coupling constants with a scaling factor large than one and extracting high-resolution spectra under inhomogeneous fields, the techniques proposed herein may be used in localized spectroscopy for improving prior knowledge of *J* coupling constants and chemical shifts required for spectral fitting and *in situ* analysis of chemical systems. The low SNR and sensitivity of iMQC signals compared to conventional SQCs remains an issue for potential applications. Improved experimental conditions such as higher magnetic fields will partially remedy the issue. Based on the similar concepts, design of new pulse sequences is under way to obtain apparent *J* coupling constants with a scaling factor small than one for spectral simplification of strongly coupled spin systems.

Acknowledgments

This work was partially supported by the NNSF of China under Grants 20573084 and 10575085, and the US NIH under Grant NS41048.

References

[1] K.M. Koch, P.B. Brown, D.L. Rothman, R.A. de Graaf, Sample-specific diamagnetic and paramagnetic passive shimming, J. Magn. Reson. 182 (2006) 66–74.
[2] J. Shen, D.L. Rothman, Fast automatic adjustment of on-axis shims for high-resolution NMR, J. Magn. Reson. 127 (1997) 229–232.
[3] J. Perlo, F. Casanova, B. Blümich, *Ex situ* NMR in highly homogeneous fields: ^{1}H spectroscopy, Science 315 (2007) 1110–1112.
[4] J. Perlo, V. Demas, F. Casanova, C.A. Meriles, J. Reimer, A. Pines, B. Blümich, High-resolution NMR spectroscopy with a portable single-sided sensor, Science 308 (2005) 1279.
[5] R.A. de Graaf, D.L. Rothman, K.L. Behar, High resolution NMR spectroscopy of rat brain *in vivo* through indirect zero-quantum-coherence detection, J. Magn. Reson. 187 (1997) 320–326.
[6] W.S. Warren, W. Richter, A.H. Andreotti, B.T. Farmer II, Generation of impossible cross-peaks between bulk water and biomolecules in solution NMR, Science 262 (1993) 2005–2009.
[7] C.A. Corum, A.F. Gmitro, Spatially varying steady state longitudinal magnetization in distant dipolar field-based sequences, J. Magn. Reson. 171 (2004) 131–134.
[8] C.A. Corum, A.F. Gmitro, Visualizing distant dipolar field and intermolecular multiple quantum coherence sequences, in: Proceedings of the International Society of Magnetic Resonance in Medicine 12th Scientific Meeting, Kyoto, 2004, p. 2711.
[9] S. Datta, S.Y. Huang, Y.Y. Lin, Contrast enhancement by feedback fields in magnetic resonance imaging, J. Phys. Chem. B 110 (2006) 22071–22078.
[10] S. Vathyam, S. Lee, W.S. Warren, Homogeneous NMR spectra in inhomogeneous fields, Science 272 (1996) 92–96.
[11] Y.Y. Lin, S. Ahn, N. Murali, W. Brey, C.R. Bowers, W.S. Warren, High-resolution, >1 GHz NMR in unstable magnetic fields, Phys. Rev. Lett. 85 (2000) 3732–3735.
[12] G. Galiana, R.T. Branca, W.S. Warren, Ultrafast intermolecular zero quantum spectroscopy, J. Am. Chem. Soc. 127 (2005) 17574–17575.
[13] Z. Chen, T. Hou, Z.W. Chen, D.W. Hwang, L.P. Hwang, Selective intermolecular zero-quantum coherence in high-resolution NMR under inhomogeneous fields, Chem. Phys. Lett. 386 (2004) 200–205.
[14] Z. Chen, Z.W. Chen, J.H. Zhong, High-resolution NMR spectra in inhomogeneous fields via IDEAL (Intermolecular Dipolar-Interaction Enhanced All Lines) method, J. Am. Chem. Soc. 126 (2004) 446–447.
[15] D. Balla, C. Faber, Solvent suppression in liquid state NMR with selective intermolecular zero-quantum coherences, Chem. Phys. Lett. 393 (2004) 464–469.
[16] C. Faber, Solvent-localized NMR spectroscopy using the distant dipolar field: A method for NMR separations with a single gradient, J. Magn. Reson. 176 (2005) 120–124.
[17] R.V. Hosur, Scaling in one and two dimensional NMR spectroscopy in liquids, Prog. Nucl. Magn. Reson. Spectrosc. 22 (1990) 1–53.
[18] S. Heikkinen, H. Aitio, P. Permi, R. Folmer, K. Lappalainen, I. Kilpelainen, *J*-multiplied HSQC (MJ-HSQC): A new method for measuring $^{3}J(H_{N}H_{\alpha})$ couplings in ^{15}N-labeled proteins, J. Magn. Reson. 137 (1999) 243–246.
[19] Y.L. Xia, X.M. Kong, N. Ip, G. Zhu, A *J*-multiplied HMQC (MJ-HMQC) experiment for measuring $^{3}J_{HNH\alpha}$ coupling constants, J. Magn. Reson. 146 (2000) 228–231.
[20] S. Bourg, J.M. Nuzillard, In-phase double selective excitation of coupled spin systems using excitation sculpting, J. Magn. Reson. 133 (1998) 173–176.
[21] F. Rastrelli, A. Bagno, Selective *J*-resolved spectra: A double pulsed field gradient spin-echo approach, J. Magn. Reson. 182 (2006) 29–37.
[22] L. McIntyre, R. Freeman, Accurate measurement of coupling constants by *J* doubling, J. Magn. Reson. 96 (1992) 425–431.
[23] A. Garza-Garcia, G. Ponzanelli-Velazquez, F. del Rio-Portilla, Deconvolution and measurement of spin–spin splittings by modified *J* doubling in the frequency domain, J. Magn. Reson. 148 (2001) 214–219.
[24] J.C. Cobas, V. Constantino-Castillo, M. Martin-Pastor, F. del Rio-Portilla, A two-stage approach to automatic determination of ^{1}H NMR coupling constants, Magn. Reson. Chem. 43 (2005) 843–848.
[25] S. Appelt, H. Kuhn, F.W. Hasing, B. Blümich, Chemical analysis by ultrahigh-resolution nuclear magnetic resonance in the Earth's magnetic field, Nat. Phys. 2 (2006) 105–109.
[26] R.R. Ernst, G. Bodenhausen, A. Wokaun, Principles of Nuclear Magnetic Resonance in One and Two Dimensions, Clarendon Press, Oxford, 1987.
[27] C.B. Cai, Z. Chen, S.H. Cai, J.H. Zhong, A simulation algorithm based on Bloch equations and product operator matrix: Application to dipolar and scalar couplings, J. Magn. Reson. 172 (2005) 242–253.
[28] V. Govindaraju, K. Young, A.A. Maudsley, Proton NMR chemical shifts and coupling constants for brain metabolites, NMR Biomed. 13 (2000) 129–153.